Role of Entanglement Couplings in Threshold Fracture of a Rubber Network

K. A. Mazich* and M. A. Samus

Polymer Science Department, Ford Motor Company, PO Box 2053, Dearborn, Michigan 48121-2053. *Received July 19, 1989; Revised Manuscript Received November 3, 1989*

ABSTRACT: Fracture of a network under threshold conditions, i.e., fracture at infinitely long time, is governed by the length of some characteristic elastically active strand. The threshold fracture energy, τ_o, is related to this strand length through $\tau_o \propto \zeta^{1/2}$, where ζ is the number of units in the strand. Measurements of τ_o for a poly(dimethylsiloxane) (PDMS) network gave $\zeta \simeq 143$ monomer units. This strand length compares well with the entanglement spacing for PDMS ($M_e \simeq 135$ monomer units). Characterization of the network with statistical theory indicated that the average length of a strand between active chemical junction points was 1900 monomer units. Therefore, approximately 14 entanglement couplings were trapped between active chemical junctions in the network. Our results show that entanglement couplings dominate the process of fracture under threshold conditions for a network with a relatively large number of trapped entanglement interactions.

Entanglements have profound effects on the viscoelastic response of polymer systems.[1] They are found in systems of long linear chains, where neighboring molecules permeate regions occupied by other chains in the system. Overlapping chains physically entangle with each other and restrict the relative motion of large segments of neighboring chains. Chain reconfiguration for lengths greater than a critical scale, defined as the entanglement molecular weight (M_e), is retarded to longer times due to the physical entanglements between neighboring chains. Relaxations on scales smaller than M_e are apparently unaffected by the presence of the entanglements.

Several accounts of the nature of entanglements have appeared in the recent literature.[2-4] The most satisfying idea treats the restrictions imposed by entanglements in a distributed fashion. That is, the entanglements do not act at specific locations along the chains in the system. Rather, neighboring chains are thought to form a mesh, or tube, that restricts lateral movement and allows one-dimensional diffusion in the tube as a mechanism for relaxation. This theory, and several of its modifications,[5] appears to capture the essential features of experimental observations.

Recent theoretical and experimental work has also shown that entanglement couplings can dominate the small-strain equilibrium modulus of a cross-linked rubber network.[6-9] The network is formed by covalently linking together the chains of an entangled, linear system. In the process, a fraction of the entanglements present in the linear system before cross-linking are trapped between the chemically bound junction points in the network. Statistical theories have been developed to calculate the fraction of entanglements that are trapped in this process and to help quantify the contribution of trapped entanglements to the equilibrium modulus.[10,11]

Other ideas on network elasticity have treated the effects of junction fluctuations on the elastic modulus.[12,13] Topological constraints only help suppress junction fluctuation in these theories while the reduced configurations available to entangled chains is specifically neglected. Suitable choice of a parameter governing junction suppression can model elastic properties in tension and compression.[14] However, studies using theories that empirically allow contributions from junction fluctuations and entanglements show that entanglements can account for 20% to almost 90% of the linear elastic modulus, depending on the degree of entanglement in the system.[6-8]

In our work, we try to understand the role of entanglements in the threshold fracture of a rubber network. In the process of fracture, segments of network chains in the path of an advancing crack are extended to rupture at some characteristic rate. The length of the chain segment that spans the plane of the crack ought to reflect the time available for chain reconfiguration during crack propagation, much like the chain reconfigurations observed in small-strain mechanical testing. In fact, master curves of fracture (or tearing) energy can be constructed with the same shift factors that are used to superpose small-strain mechanical properties.[15,16] Drawing an analogy between fracture and small-strain mechanical properties, we expect only local chain reconfigurations over the time available for crack propagation during rapid fracture. For slow fracture, we expect that large segments of chains will be able to reconfigure over the longer times that are available to the system. Consequently, entanglement couplings should have a strong influence on the process of slow fracture through the rubber network.

Here, we focus on the length of chain segment responsible for fracture under threshold conditions. This amounts to studying fracture at infinitely long time, where all losses associated with chain deformation are neglected. As such, threshold fracture reflects only the extension to rupture of elastically active segments in the network. In our work, we compare the average chain length extended to rupture with the entanglement spacing of the system (M_e) and with other structural features of the network to determine the role of trapped entanglements in the process of threshold fracture.

Threshold Fracture Energy. We use a theory proposed by Lake and Thomas[17] to relate threshold fracture energy to the structural features of the network. This is analogous to theories that connect the small-strain equilibrium modulus to the number density of elastically active strands, γ, and the number density of elastically active junctions, μ. Following Lake and Thomas[17] and referring to Figure 1, we consider an elastically active strand that spans the plane of the crack. This strand is ζ units long, where a unit can refer to a main-chain bond, and each unit stores its dissociation energy, U. The length, ζ, is left unspecified at this point. It follows that the

0024-9297/90/2223-2478$02.50/0

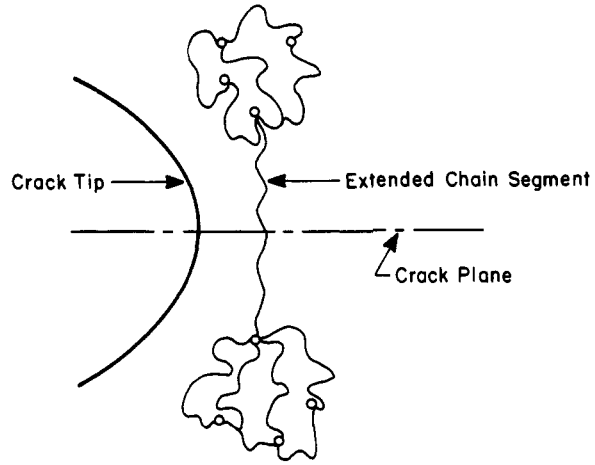

Figure 1. Schematic of an extended chain in the path of an advancing crack.

total energy required to rupture the strand is ζU, since each unit in the strand must be strained to rupture before the strand will break. For a sufficiently long strand (obeying Gaussian statistics), the end-to-end distance of the strand is $\beta\zeta^{1/2}l$, where l is the step length and β accounts for deviations from a freely jointed chain. The number of strands that cross a unit area in the network is $\gamma\beta\zeta^{1/2}l/2$. Thus, the threshold fracture energy, τ_0, defined as the stored energy released per unit area of crack surface created is

$$\tau_0 \propto \gamma(\zeta)\zeta^{1.5} \tag{1}$$

Specific definitions of ζ lead to relations between τ_0 and structural features of the network. For instance, writing $\gamma = \rho N_A/M_c$, where M_c is the molecular weight between chemical junctions and ρ is the density, gives a familiar form of the Lake–Thomas theory:[15,17-22]

$$\tau_0 \propto M_c^{1/2} \tag{2}$$

Various experimental studies have verified the form of the Lake–Thomas theory as expressed in eq 2.[17-22] τ_0 for both end-linked and randomly linked networks followed the power law form given above. The Lake–Thomas theory was also used to study the unusual toughness of an end-linked network prepared with a bimodal distribution of parent chain lengths.[21,23-25] In the studies cited here, M_c for end-linked networks was equated to the molecular weight of the parent polymer chains, and randomly linked networks were characterized by calculating M_c from the Mooney–Rivlin constant, C_1. In virtually every study, networks were prepared such that $M_c < M_e$. Networks with this characteristic have very few, if any, trapped entanglements.

Other definitions of ζ in eq 1 can account for the contribution of trapped entanglements to the threshold fracture energy. Here, we let ζ equal the spacing between chemical junctions and entanglement points. Following the Graessley–Langley[6,7,10] approach for the small-strain equilibrium modulus, we assume that the contributions of chemical junctions and trapped entanglements to elastically active network structures are additive. The expression for ζ becomes

$$\zeta = \rho/2m_0(\mu_c + T_e\mu_e) \tag{3}$$

where μ_e is the maximum number density of entanglement points in the network, T_e is the fraction of entanglements that are trapped by elastically active junctions, and m_0 is the monomer molecular weight. Considering tetrafunctional junctions and setting $T_e = 1$, τ_0 becomes

$$\tau_0 \propto (1/M_c + 1/M_e)^{-1/2} \tag{4}$$

For loosely cross-linked networks, $M_c \gg M_e$, and, from eq 4, we expect that τ_0 will be a constant proportional to $M_e^{1/2}$.

Network Characterization. Our analysis of the structural components of a randomly linked network makes use of a theory given by Pearson and Graessley.[11] Through statistical arguments, they were able to calculate the average length of various structural parameters in a multifunctional network. With this analysis, we circumvent the characterization of elastically active chains with the Mooney–Rivlin constant, C_1. Applicable results of their development can be found in ref 11.

Experimental Materials and Methods

A sample of commercial, high molecular weight poly(dimethylsiloxane) (PDMS) was supplied by Dow Corning (Silastic 4-2736) for this study. The repeat unit can be represented as $[Si(CH_3)_2O]$. The high degree of flexibility and thermal stability of PDMS allow an easier, more accurate measurement of τ_0, since energy losses are minimized at experimentally accessible temperatures.

An analysis of the primary molecular weight distribution of Silastic 4-2736 was performed with gel permeation chromatography. PDMS standards purchased from the American Polymer Standards Corp. (Mentor, OH) (molecular weight ranged from 40 000 to 680 000) and polystyrene (PS) standards supplied by Waters (Milford, MA) (molecular weight ranged from 2000 to 2 000 000) were used to construct a calibration curve. Elution times for PS standards above M = 700 000 and below M = 40 000 (where M is molecular weight) were used to extend the range of molecular weight encompassed by the calibration curve. The coincidence of PDMS and PS calibration curves at high and low molecular weights, respectively, justified this approach.

A small sample of Silastic 4-2736 was passed through a two-roll mill for the same period of time that was used to mix PDMS with curing agent. GPC analysis of the milled sample identified a small amount of low molecular weight material. Neglecting the low molecular weight tail, GPC analysis gave M_w/M_n = 592 000/400 000.

Network Preparation. A bisperoxide, 1,4-bis(2-*tert*-butylperoxyisopropyl)benzene, supplied by Noury Chemical (Perkadox 14) was chosen to cure PDMS. 1 phr (parts per hundred rubber, by weight) Perkadox 14 was mixed with 100 phr PDMS on a small two-roll mill at room temperature. The compound was allowed to relax in a sealed container at room temperature for approximately 7 days to allow the mechanically entrapped air to escape. The material was then cut into 30-g samples ca. 190 mm × 30 mm for pure shear specimens and 45-g samples of 160 mm × 160 mm × 2 mm for standard ASTM slabs. The specimens were press cured for 15 min at 170 °C, followed by an air oven postcure of 24 h at 200 °C. A fluorocarbon mold release was used along the edges of the molds to facilitate removal of the specimens.

Linear Viscoelastic Properties. The linear viscoelastic properties of cross-linked PDMS were measured with a Rheometrics Mechanical Spectrometer Model 800 (RMS-800). A circular disk of material 25 mm in diameter was cut from the ASTM slab and mounted between parallel plates at room temperature. Sample thickness was approximately 2 mm. The dynamic moduli in shear, G' and G'', were measured for a range of strain amplitude from 0.1% to 50% at 10 rad/s. From this data, we determined that linear properties could be measured to 5% strain. Since the stiffness of the sample and geometry yielded rather small torques, we used 5% strain in all subsequent experiments to ensure linearity while generating the greatest possible torque signal.

The RMS-800 contains a normal force transducer that helps the instrument compensate for thermal expansion or contraction of the sample and fixtures. We calibrated the change in the fixture zero with temperature, and we applied a suitable

correction for gap height to the data collected at temperatures other than the mounting temperature (room temperature). Raw data were multiplied by the ratio of corrected gap height to uncorrected gap height.

Sol Fraction Analysis. A small sample of cross-linked PDMS from the gauge section of a pure shear specimen was swollen in an excess of toluene at room temperature to extract the sol fraction. The solvent was replaced with fresh toluene every 7 days. Old solvent, containing some of the extracted sol, was collected after each exchange. Four solvent changes were performed before the swollen PDMS sample was dried to constant weight. The procedure was repeated until the dried sample weight agreed with the dry weight of the previous extraction to within 0.001 g. The gel fraction, calculated with the final weight of the dried sample, equaled 0.894 of the original weight.

We confirmed the value of the gel fraction by removing toluene from the combined extracted solution with a rotary evaporator. The dried, extracted material accounted for 0.106 of the original sample weight.

Mechanical Properties at Moderate Strains. An Instron servohydraulic testing machine, Model 1350, was used to measure the stress relaxation of PDMS under moderate strains in pure shear. Methods are described elsewhere.[26] The data were fit with an empirical relation proposed by Chasset and Thirion[27,28] to describe stress relaxation of cross-linked rubbers at long times

$$\sigma = \sigma_0[1 - (t/t_m)^{-m}] \quad (5)$$

where t_m is a single characteristic time for long-time relaxation and σ_0 is the equilibrium stress in the material.

An "equilibrium" stress–strain diagram was constructed by calculating the stress at $t = 10^5$ s with eq 5 and plotting against the deformation ratio, λ. Time $t = 10^5$ s was chosen because this time is a more realistic representation of the time scale of our fracture experiments that are described below. The strain energy density, W, was calculated from the area under the stress–strain plot.

Fracture Energy. After collecting stress relaxation data in pure shear, samples were used to measure the fracture energy of cross-linked PDMS as a function of crack growth rate. A cut approximately 20 mm in length was introduced into one edge of the sample, roughly midway between the grips. A very small deformation was applied to observe the cut, and the initial crack length was measured with a cathetometer. A step strain was then applied to the specimen, and the crack was allowed to propagate a certain perceptible distance. The time increment was recorded, and the crack length was measured. A linear fit through the crack length vs time data produced the crack growth rate at the given strain of the experiment.

Fracture energy was calculated with the strain energy density in the bulk of the sample, W, and the undeformed height of the sample, h_0:[29]

$$\tau = Wh_0 \quad (6)$$

In the derivation of eq 6, we assume that a volume of material equal to $th_0\delta a$ (for thickness, t) passes from the bulk deformed state to the completely relaxed state as the crack length increases by δa.[29]

Results and Discussion

Statistical Characterization of the Network. Statistical arguments given by Pearson and Greassley[11] can be used to calculate structural features of the PDMS network. From GPC analysis, the number average number of units per chain, r_n, is 5405 units per chain and the weight average number of units per chain, r_w, is 8000 units per chain. Extraction of the network gave $s = 0.106$. These experimental results were used with expressions found in ref 11 to calculate the network parameters listed in Table I.

The fraction of cross-linked units in the network, α, can be compared with the critical fraction of cross-linked units necessary for gel formation, α_c. Following Flory,[30] $\alpha_c \simeq 1/r_w = 1.25 \times 10^{-4}$. Comparing $\alpha/\alpha_c \simeq 4$, we find that the PDMS network contains approximately

Table I

sol fraction, s	0.106
fraction of cross-linked units, α	4.62×10^{-4}
active strands/cm^3, γ	1.69×10^{18}
active junctions/cm^3, μ	1.02×10^{18}
entanglement trapping factor, T_e	0.165
units/active strand, L	1900

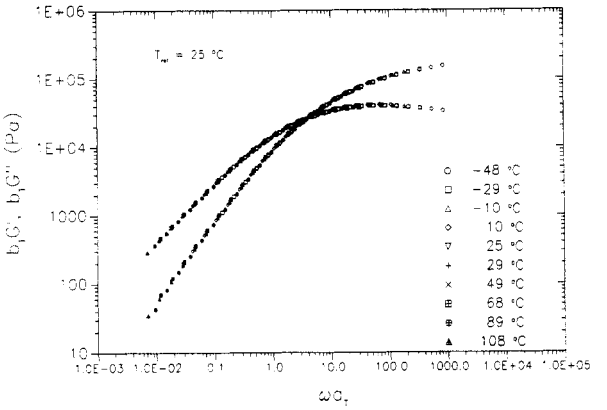

Figure 2. Master curves of G' and G'' for a PDMS melt. Reference $T = 25$ °C.

4 times as many cross-links as are necessary to form a gel.

The number of units in an elastically active strand, L, is a direct measure of the spacing between chemically bound junction points in the network. When the possible role of trapped entanglements between the chemical junctions is neglected, this parameter should reflect the maximum possible extension that the network can absorb before rupture. From Table I, we find that, on average, 1900 PDMS monomer units form an elastically active strand between chemical junctions. This spacing can be compared with the number of units between entanglement points. With $M_e \simeq 10\,000$, found from the linear viscoelastic measurements discussed in the following section, and $m_0 = 74$, the spacing between entanglement points is 10 000/74, or 135 monomer units, and 1900/135, or approximately 14, entanglement couplings are trapped between chemical junctions along an elastically active strand.

Linear Viscoelastic Properties. A characterization of the linear viscoelastic properties of the PDMS network was performed to complement the statistical calculations of network structure discussed above. The storage modulus (G') and loss modulus (G'') in simple shear for the parent PDMS melt and the cross-linked PDMS network were measured from 0.01 to 100 rad/s at temperatures from −48 to +108 °C for the melt and from −32 to +84 °C for the network. The strong curvatures of G' and G'' with frequency for the melt allow an accurate application of the time–temperature superposition principle.[31]

The master curve for the PDMS melt with reference $T = 25$ °C is presented in Figure 2. In the plateau region above 10 rad/s, G' and G'' vary slowly with frequency. An estimate of the plateau modulus, G_N, for the melt can be calculated from this data with eq 7[31] if the upper

$$G_N = \frac{2}{\pi}\int_{-\infty}^{c} G'' \, d \ln w \quad (7)$$

integration limit, c, can be chosen such that the entanglement peak converges to zero before entering the transition zone. Using eq 7, we estimate $G_N \simeq 0.24$ MPa and M_e (or $\rho RT/G_N$) $\simeq 10\,000$. This estimate of the

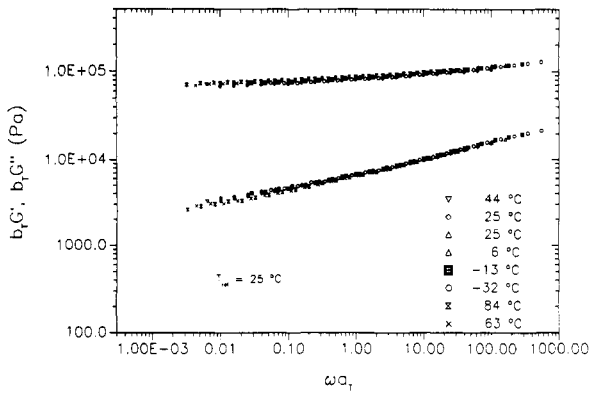

Figure 3. Master curves of G' and G'' for a PDMS network. Reference T = 25 °C.

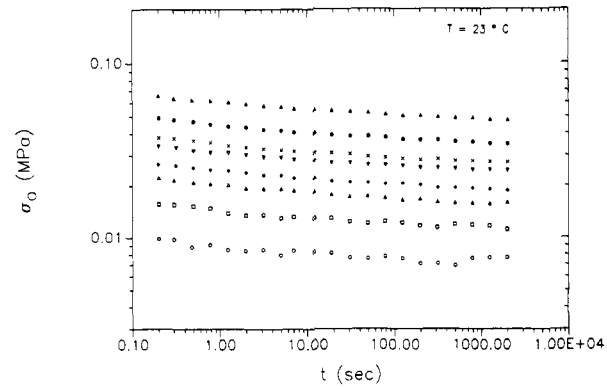

Figure 4. Stress relaxation curves for a PDMS network at 23 °C. Deformation ratios are listed as follows: (▲) 1.30, (●) 1.20, (×) 1.15, (▽) 1.125, (◆) 1.10, (△) 1.08, (□) 1.05, (○) 1.03.

entanglement spacing compares favorably with values for M_e found in the literature.[1,32]

Master curves for the cross-linked PDMS sample, presented in Figure 3, were constructed with shift factors found from the analysis of melt data. From the low-frequency limit of G', we estimate the equilibrium shear modulus of the network, G_o = 0.065 MPa. This estimate can be compared with the Graessley–Langley[6,7,10] form for G_o. Contributions from chemical junctions and trapped entanglements add to give G_o:

$$G_o = (\gamma - h\mu)kT + T_e G^{max} \quad (8)$$

The first term in eq 11 is the contribution of active strands between chemically bound junctions. It has the form of phantom network theory, where h is an empirical factor ($0 < h < 1$) that accounts for junction fluctuations. The second term is the trapped entanglement contribution, where T_e is the trapping factor and G^{max} is the maximum possible contribution of entanglements to G_o. Experimental results for a variety of networks indicate that G^{max} is approximately equal to G_N.[6-9] With $G^{max} \simeq G_N$ and h = 0, we calculate G_o = 0.047 MPa. This compares well with the estimate of G_o from the low-frequency limit of G'. The agreement of G_o from viscoelastic measurements with the form of the Graessley–Langley theory verifies the role of entanglement couplings in small-strain mechanical properties of the network. In fact, the entanglement term in eq 8 accounts for 85% of the calculated modulus.

An estimate of the number of trapped entanglement couplings per elastically active strand can also be found with the equilibrium shear modulus. We define γ^* as the density of active strands joined by chemical junctions and trapped entanglements. Using the Graessley–Langley form for G_o and assuming that junction fluctuations are totally suppressed (h = 0), we can write $\gamma^* = G_o/kT$. The average number of entanglement couplings per active strand is equal to the ratio γ^*/γ. Using γ from the statistical characterizaion of the network and γ^* from the measured shear modulus, we find $\gamma^*/\gamma \simeq$ 10 entanglement coupling per active strand. This calculation compares well with the purely statistical result of 14 entanglement couplings per active strand. From this comparison, we can conclude that entanglement couplings outnumber chemical junctions by about a factor of 10.

Stress–Strain Properties at Moderate Strain. A series of stress relaxation experiments in pure shear were performed to determine the equilibrium stress as a function of strain at moderate deformations. Representative experimental results at 23 °C are shown in Figure 4. Stress decays approximately 30% over the time interval of the experiment at 23 °C and approximately 20% at 100 °C.

The data in Figure 4 also appear to follow the same time dependence for all values of the deformation ratio, λ. This result implies that the effects of time and strain are separable and that the stress can be represented with

$$\sigma(\lambda,t) = h(\lambda)\, g(t) \quad (9)$$

The time-dependent function can be expressed with an empirical relation for long-time relaxation in networks due to Chasset and Thirion:[27,28]

$$g(t) = 1 - (t/t_m)^{-m} \quad (10)$$

A fit of the stress relaxation data with eq 10 gave m = 0.15 and $t_m = 10^{-6}$ at 23 °C and m = 0.18 and t_m = 5.7 × 10^{-6} at 100 °C.

The stress used for the fracture analysis is calculated from eq 10 at $t = 10^5$ s. This is a good estimate of the time scale for the fracture experiments discussed below. Stress at $t = 10^5$ s based on initial cross-sectional area was plotted against λ, as shown in Figure 5. Fitting functions for the data were analytically integrated to calculate the strain energy density, W.

Fracture. In a series of fracture experiments on cross-linked samples, we measured the threshold fracture energy, τ_o, of the PDMS network. Experiments were conducted at very slow crack growth rates, or long times, and a limiting value of fracture energy at infinite time represented the threshold fracture energy.

Pure shear specimens were cut with a scalpel at one edge and deformed to a given value of λ (measured in the bulk section of the sample, far from the crack tip). The crack length, measured in the undeformed state, was recorded as a function of time, and crack growth rates, $\dot{a}$, were found from the slope of these data. Sample data are presented in Figure 6 for λ = 1.14 at 100 °C, indicating that crack length varies linearly with time. Similar results were found in all of the fracture experiments.

Fracture energy, τ, calculated with eq 6, is plotted against $\dot{a}$ in Figure 7. Data at 23 and 100 °C show a definitive rate dependence above 10^{-4} mm/s but appear to approach a limiting value as the rate decreases. In some experiments, the sample was left in the deformed state, corresponding to some value for τ, for at least 24 h without any perceptible increase in the length of the crack. These points, plotted on the τ axis in Figure 7, lie near the limiting value for τ obtained by extrapolating the data to long times.

In addition, fracture energies for the two temperatures were shifted along the rate axis in an attempt to superpose the data (Figure 8). The shift factor that we

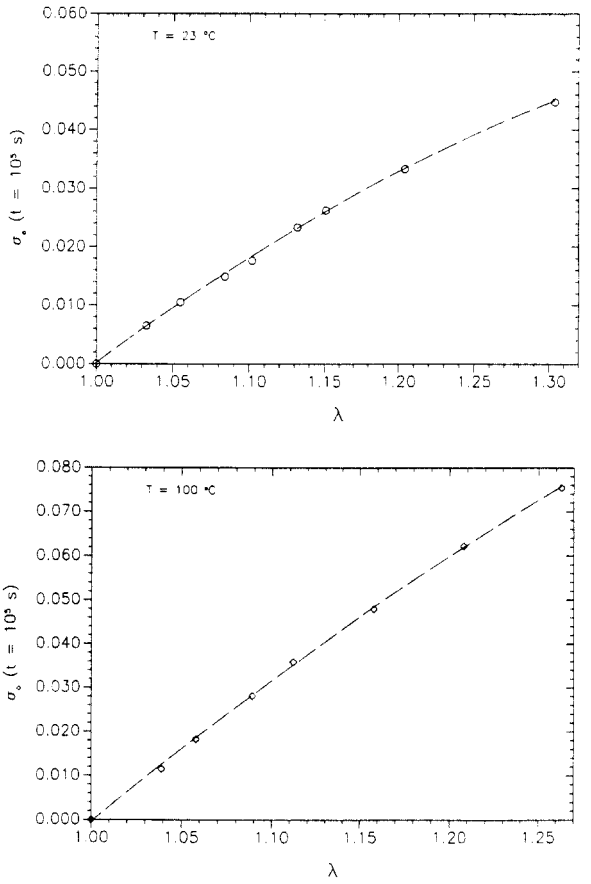

Figure 5. Stress (based on initial cross-sectional area) vs deformation ratio. Top curve for 23 °C. Bottom curve for 100 °C.

used is the same shift factor used to superpose G' and G''. The success of this superposition technique implies that the time scales of viscoelastic processes that operate under the small strains of the linear viscoelastic experiments are also responsible for the large strain processes that operate in fracture of the network. The shifted data in Figure 8 clearly show the limiting region of the fracture energy. From this data, we chose $\tau_o = 0.029$ N/mm.

This result for the threshold fracture energy was used with the Lake–Thomas theory to calculate the effective strand length for fracture under threshold conditions. Defining ζ^* as the number of main-chain atoms in this effective strand length for fracture and noting that $\gamma = \rho N_A/q\zeta^*$ (where q is the monomer molecular weight per main-chain atom), we can rearrange eq 1 to solve for ζ^*, as shown in

$$\zeta^* = [2q\tau_o/\beta U l \rho N_A]^2 \qquad (11)$$

Substituting for PDMS[21] ($\beta = 2.5$, $U = 6.1 \times 10^{-19}$ J, $l = 0.143 \times 10^{-9}$ m, and $q = 37$ g/mol), this expression gives $\zeta^* \simeq 286$ main-chain atoms. Since PDMS has two main-chain atoms per monomer, $\zeta = \zeta^*/2$ or 143 monomer units comprise the effective chain for threshold fracture. Comparing ζ with the average entanglement spacing (135 monomer units), we conclude that the chain length between entangled points along elastically active strands is responsible for threshold fracture.

This result is interesting to compare with our calculation of 14 entangled subchains between chemical junction points in the PDMS network. The high number of trapped entanglements relative to the number of chemical junctions ($M_c \gg M_e$) apparently dictates that the properties of the network are largely governed by entanglement spacings. Both G_o and τ_o, properties at small strain and large strain, respectively, depend primarily on

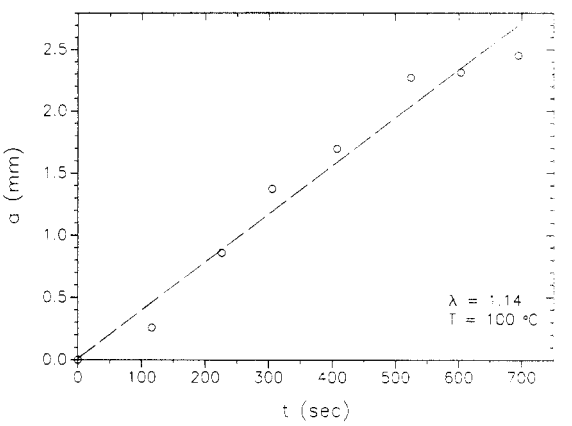

Figure 6. Crack length, a, vs time at 100 °C and $\lambda = 1.14$.

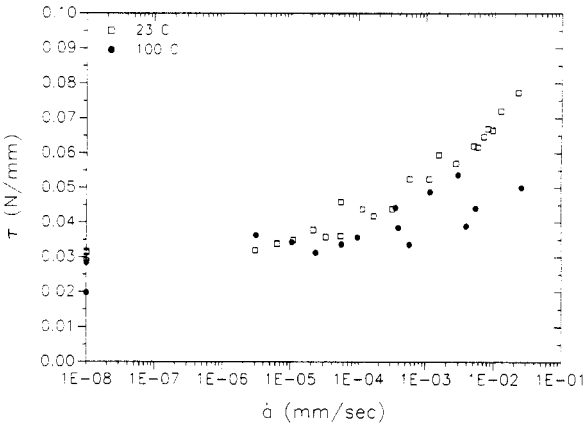

Figure 7. Fracture energy, τ, vs crack growth rate, $\dot{a}$: (□) 23 °C; (●) 100 °C.

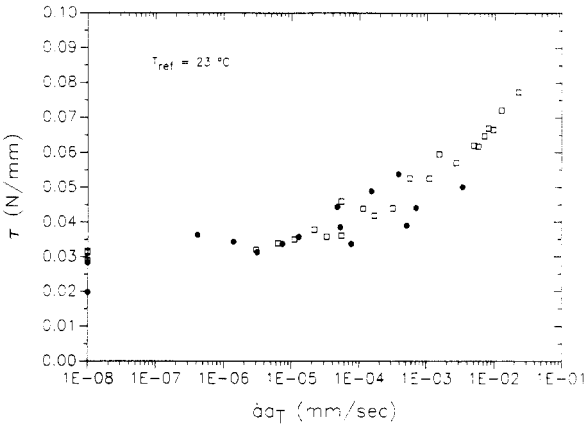

Figure 8. Master curve for the fracture energy, τ. Reference $T = 23$ °C.

trapped entanglement couplings in this network. The fact that ζ is on the order of the entanglement spacing suggests that trapped entanglements do not slip along active strands, even as the network is strained to a very large degree.

The conclusions given here extend the interpretation of threshold fracture data to loosely cross-linked networks with $M_c \gg M_e$. Much of the earlier work on threshold fracture has shown that $\tau_o \simeq M_c^{1/2}$ for networks with $M_c < M_e$.[17-22] Sample data presented by Gent and Tobias[18] on a series of randomly cross-linked and end-linked PDMS networks verify the $M_c^{1/2}$ dependence for τ_o when $M_c < 10\,000$. However, a single data point above $M_c \simeq 10\,000$ ($=M_e$) suggests that τ_o approaches some constant value for networks with $M_c > 10\,000$. Similar observations were made by Ahagon and Gent[22] on a series of polybutadiene networks. These experimental results

are consistent with the view that τ_o depends on M_e for a network with $M_c \gg M_e$.

Another important example of threshold fracture data for a network with $M_c \simeq M_e$ also supports this conclusion. Working with an end-linked PDMS network with a parent chain molecular weight approximately equal to M_e (M_n = 6800), Yanyo and Kelley[21] measured τ_o = 0.03 N/mm. The numerical agreement of τ_o for this end-linked network with our measurement of τ_o for a lightly cross-linked network implies that the elastically active chain lengths in threshold fracture for the two networks were comparable.

Conclusions

The threshold fracture energy measured for a cross-linked PDMS network was 0.029 N/mm. With the Lake–Thomas theory for fracture under threshold conditions, we found that the average network subchain that is extended to the breaking point under threshold conditions is approximately 140 monomer units in length. This subchain length compares very well with the subchain length between entanglements found from a linear viscoelastic characterization of the network (approximately 135 monomer units). We conclude that entangled subchains trapped by chemical junctions along elastically active strands are responsible for threshold fracture. This result implies that trapped entanglement couplings do not slip along active strands as the network is pulled to its maximum extension.

We also used a statistical theory for randomly cross-linked networks to calculate the average length of elastically active subchains between chemical junction points in the network. Approximately 1900 monomer units comprise the active strand between chemical junctions. Combining this result with the entanglement spacing, we found that there are approximately 14 entangled subchains between chemical junctions. The relatively large number of entangled subchains per active chain account for the observations and conclusions given above.

References and Notes

(1) Graessley, W. W. *Adv. Polym. Sci.* **1974**, *16*, 1.
(2) Edwards, S. F. *Proc. Phys. Soc.* **1967**, *92*, 9.
(3) de Gennes, P.-G. *J. Chem. Phys.* **1971**, *55*, 572.
(4) Doi, M.; Edwards, S. F. *J. Chem. Soc., Faraday Trans. 2* **1978**, *74*, 1789, 1802, 1818.
(5) Graessley, W. W. *Adv. Polym. Sci.* **1982**, *47*, 67.
(6) Dossin, L. M.; Graessley, W. W. *Macromolecules* **1979**, *12*, 123.
(7) Pearson, D. S.; Graessley, W. W. *Macromolecules* **1980**, *13*, 1001.
(8) Gottlieb, M.; Macosko, C. W.; Lepsch, T. C. *J. Polym. Sci., Polym. Phys. Ed.* **1981**, *19*, 1603.
(9) Langley, N. R.; Polmanteer, K. E. *J. Polym. Sci., Polym. Phys. Ed.* **1974**, *12*, 1023.
(10) Langley, N. R. *Macromolecules* **1968**, *1*, 348.
(11) Pearson, D. S.; Graessley, W. W. *Macromolecules* **1978**, *11*, 528.
(12) Ronca, G.; Allegra, G. J. *J. Chem. Phys.* **1975**, *63*, 4990.
(13) Flory, P. J.; Erman, B. *Macromolecules* **1982**, *15*, 800.
(14) Erman, B.; Flory, P. J. *Macromolecules* **1982**, *15*, 806.
(15) Plazek, D. J.; Choy, I.-C.; Kelley, F. N.; von Meerwall, E.; Su, L.-J. *Rubber Chem. Technol.* **1983**, *56*, 866.
(16) Kadir, A.; Thomas, A. G. *Rubber Chem. Technol.* **1981**, *54*, 15.
(17) Lake, G. J.; Thomas, A. G. *Proc. R. Soc. London, Ser. A* **1967**, *300*, 108.
(18) Gent, A. N.; Tobias, R. H. *ACS Symp. Ser.* **1982**, *193*, 367.
(19) Gent, A. N.; Tobias, R. H. *J. Polym. Sci., Polym. Phys. Ed.* **1982**, *20*, 2051.
(20) Bhowmick, A. K.; Gent, A. N.; Pulford, C. T. R. *Rubber Chem. Technol.* **1983**, *56*, 226.
(21) Yanyo, L. C.; Kelley, F. N. *Rubber Chem. Technol.* **1987**, *60*, 78.
(22) Ahagon, A.; Gent, A. N. *J. Polym. Sci., Polym. Phys. Ed.* **1975**, *13*, 1903.
(23) Llorente, M. A.; Andrady, A. L.; Mark, J. E. *J. Polym. Sci., Polym. Phys. Ed.* **1981**, *19*, 621.
(24) Zhang, Z. M.; Mark, J. E. *J. Polym. Sci., Polym. Phys. Ed.* **1982**, *20*, 473.
(25) Mark, J. E.; Andrady, A. L. *Rubber Chem. Technol.* **1981**, *54*, 366.
(26) Sullivan, J. L.; Demery, V. C. *J. Polym. Sci., Polym. Phys. Ed.* **1982**, *20*, 2083.
(27) Chasset, R.; Thirion, P. *Proceedings of the Conference on the Physics of Non-Crystalline Solids*; Prins, J. A., Ed.; North-Holland Publishing: Amsterdam, 1965; p 345.
(28) Curro, J. G.; Pincus, P. *Macromolecules* **1983**, *16*, 559.
(29) Rivlin, R. S.; Thomas, A. G. *J. Polym. Sci.* **1953**, *10*, 291.
(30) Flory, P. J. *Principles of Polymer Chemistry*; Cornell University Press: Ithaca, NY, 1953.
(31) Ferry, J. D. *Viscoelastic Properties of Polymers*, 3rd ed.; John Wiley and Sons, Inc.: New York, 1980.
(32) Langley, N. R.; Ferry, J. D. *Macromolecules* **1968**, *4*, 353.